

Federated nnU-Net for Privacy-Preserving Medical Image Segmentation

Grzegorz Skorupko*¹, Fotios Avgoustidis*¹, Carlos Martín-Isla¹, Lidia Garrucho¹, Dimitri A. Kessler¹, Esmeralda Ruiz Pujadas¹, Oliver Díaz¹, Maciej Bobowicz², Katarzyna Gwoździwicz², Xavier Bargalló³, Paulius Jaruševičius⁴, Kaisar Kushibar¹, and Karim Lekadir^{1,5}

¹Artificial Intelligence in Medicine Laboratory (BCN-AIM), Departament de Matemàtiques i Informàtica, Universitat de Barcelona, Spain

²Medical University of Gdańsk (GUMed), Poland

³Hospital Clínic de Barcelona (HCB), Spain

⁴Lithuanian University of Health Sciences, Lithuania

⁵Institució Catalana de Recerca i Estudis Avançats (ICREA), Spain

March 5, 2025

Abstract

The nnU-Net framework has played a crucial role in medical image segmentation and has become the gold standard in multitudes of applications targeting different diseases, organs, and modalities. However, so far it has been used primarily in a centralized approach where the data collected from hospitals are stored in one center and used to train the nnU-Net. This centralized approach has various limitations, such as leakage of sensitive patient information and violation of patient privacy. Federated learning is one of the approaches to train a segmentation model in a decentralized manner that helps preserve patient privacy. In this paper, we propose FednnU-Net, a federated learning extension of nnU-Net. We introduce two novel federated learning methods to the nnU-Net framework – Federated Fingerprint Extraction (FFE) and Asymmetric Federated Averaging (AsymFedAvg) – and experimentally show their consistent performance for breast, cardiac and fetal segmentation using 6 datasets representing samples from 18 institutions. Additionally, to further promote research and deployment of decentralized training in privacy-constrained institutions, we make our plug-n-play framework public. The source-code is available at <https://github.com/faildeny/FednnUNet>.

data privacy, federated learning, image segmentation, nnU-Net, nnUNet

1. Introduction

Medical image segmentation plays a key role in clinical workflows to accurately delineate anatomical structures and help with diagnosis, treatment planning, and disease monitoring [1–6]. Deep learning methods, especially convolutional neural networks (CNNs), have shown great success in this field. One of the most effective approaches is the no-new-U-Net framework (nnU-Net) [7] which, over the years, has established itself as the go-to framework for medical image segmentation task, evidenced by its multiple first-place finishes on public leaderboards and its widespread adoption as the foundation for further model development across diverse segmentation challenges [8, 9]. nnU-Net extends the widely adopted U-Net architecture [10], which utilizes an encoder-decoder structure with skip connections to capture both semantic and localization information. Going beyond the original U-Net, nnU-Net automatically configures network architectures tailored to a given dataset, provides a robust training schedule and data augmentation strategy, as well as postprocessing methods to further improve the final performance. This “no-new” principle eliminates much of the manual effort associated with hyperparameter tuning and architectural engineering, rendering nnU-Net both powerful and highly convenient across a broad range of biomedical tasks [7, 11–13]. Despite these advancements, the development of robust segmentation models often requires aggregating extensive datasets from multiple institutions to capture diverse patient populations and imaging protocols. However, the consolidation of such data is frequently impeded by stringent data privacy regulations, ethical considerations, and logistical challenges associated with data sharing. Federated learning (FL) [14] has emerged as a promising solution to these challenges by facilitating collaborative model training across multiple institutions without the need to exchange raw data. Federated learning, however, presents significant challenges when data are heterogeneous across institutions. Traditional FL approaches typically assume that all participants train

This work received funding from the European Union’s Horizon Europe research and innovation programme under Grant Agreement No. 101044779 (Aimix project), Grant Agreement No. 952103 (EuCanImage project), Grant Agreement No. 101057699 (RadioVal project) and Grant Agreement No. 101057849 (DataTools4Heart project).

* These authors contributed equally to this work.

Corresponding author: Grzegorz Skorupko (grzegorz.skorupko@ub.edu).

identical models on similarly distributed data, yet in real-world scenarios, clients often have different computational resources and dataset characteristics. To address this disparity, methods such as HeteroFL [15] have been introduced to enable federated training among clients with varying model capacities, while more recent efforts [16] have focused on mitigating label noise and inconsistencies inherent in federated settings. Collectively, these approaches underscore the growing need for robust FL techniques that can simultaneously manage model and data heterogeneity. Regardless of the significant federated developments in medical domain [17–23], those methods have not been explicitly tailored for medical image segmentation tasks using nnU-Net. Moreover, nnU-Net’s plug-and-play design, which has made it the gold standard in centralized settings, no longer functions seamlessly in federated environments, necessitating tailored adaptations to overcome the challenges of decentralized, heterogeneous data. To bridge the gap between the decentralized learning paradigms and the robust capabilities of nnU-Net framework, we introduce **FednnU-Net**, federated extension of nnU-Net that enables collaborative training while preserving data privacy. To the best of our knowledge, it is the first fully-federated and privacy-preserving implementation of nnU-net. We propose two novel methods—**Federated Fingerprint Extraction (FFE)** and **Asymmetric Federated Averaging (AsymFedAvg)**. These methods address the challenges posed by variations in dataset properties across different centers, ensuring that each institution maximizes the benefit from shared knowledge training. Our experiments demonstrate that both methods consistently outperform local, non-collaborative training setups for 2D and 3D segmentation tasks across six public and non-public datasets. By extending nnU-Net’s automated pipeline to federated learning and introducing methods to handle data heterogeneity, this work aims to advance the development of robust, scalable, and privacy-preserving medical image segmentation solutions.

2. Methods

We propose two novel methods to federate nnU-Net’s pipeline for image segmentation: FFE and AsymFedAvg. These two approaches address the challenges of decentralized, heterogeneous data in model training while maintaining nnU-Net’s self-configuring advantages.

2.1. nnU-Net vs FednnU-Net

nnU-Net is a multi-stage segmentation pipeline that begins with a preparation stage, where dataset fingerprint extraction is performed and a customized training plan (including a tailored network architecture) is generated. This is followed by a training stage and concludes with a post-training stage that selects the best-performing models and optimal image post-processing techniques. To extend nnU-Net into a federated learning setting, we integrate our proposed methods at key points in this pipeline. The first method, FFE, is incorporated into the preparation stage to ensure that data characteristics from all participating institutions are captured and considered when generating the training plan. The second method, AsymFedAvg, operates during the training stage and facilitates the aggregation of model weight updates across nodes with heterogeneous architectures. The following sections provide detailed descriptions of each method. For clarity, we use the terms “node” and “client” interchangeably to refer to each institution participating in the decentralized training process, while “server” describes the coordinating agent responsible for communication and aggregation of inputs from the nodes.

2.2. Federated Fingerprint Extraction

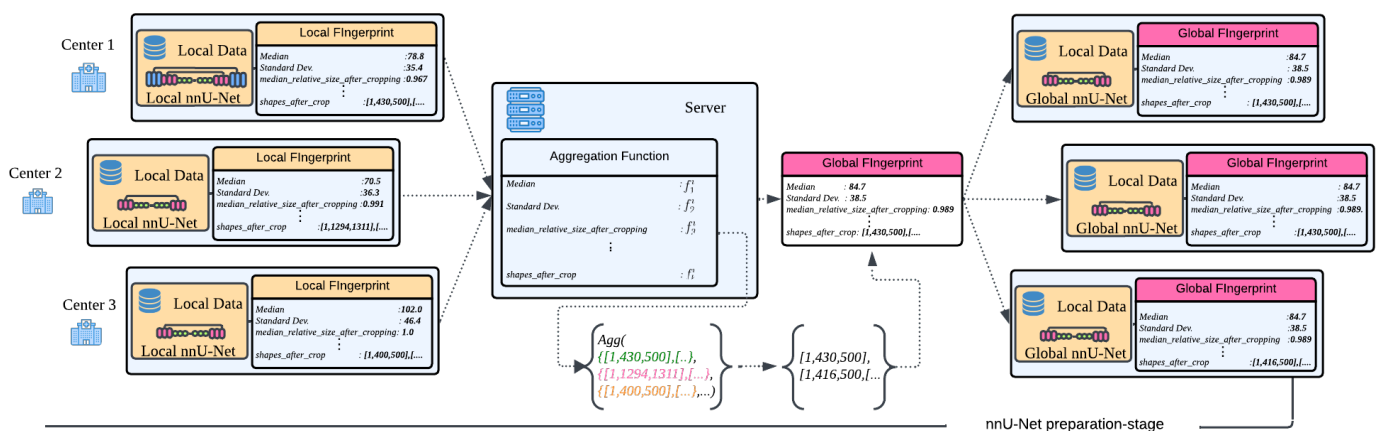


Figure 1: The Federated Fingerprint Extraction (FFE) process. Each node computes a local fingerprint from its dataset and shares it with the server, which then aggregates them into a global fingerprint. Finally, the server redistributes this global fingerprint to all nodes for local nnU-Net configuration. This process happens once at the beginning of the training stage.

Table 1: Dataset fingerprint characteristics and aggregation Functions.

Fingerprint Key	Aggregation Function g_k
<i>Pixel intensity</i>	
max	global max
min	global min
mean	weighted_mean
median	weighted_mean
std	weighted_mean
percentile_00.5	weighted_mean
percentile_99.5	weighted_mean
<i>Shape</i>	
median_relative_size_after_cropping	weighted_mean
shapes_after_crop	concatenate
spacings	concatenate

Table 2: Default nnU-Net training configurations for each center in MAMA-MIA dataset

Parameter	ISPY1	ISPY2	DUKE	NACT
2D Configuration				
Batch Size	49	32	12	49
Patch Size	[256,256]	[320,320]	[512,512]	[256,256]
Spacing	[0.78,0.78]	[0.68,0.68]	[0.70,0.70]	[0.70,0.70]
U-Net Stages	7	7	8	7
Features/Stage	[32-512]	[32-512]	[32-512]	[32-512]

The proposed FFE method enables the analysis of the federated datasets and the configuration of nnU-Net, allowing to determine a unified, one-fits-all training strategy for all data centers in the federated setup. This approach effectively approximates the configuration behaviour in a centralized environment. The dataset’s fingerprint is a crucial component of the nnU-Net’s adaptive configuration, summarizing the key dataset characteristics that are used to determine the model configuration and preprocessing strategies. The FFE approach comprises two key steps:

- **Local Fingerprint Extraction:** Each participating node generates their dataset fingerprint by invoking the extraction process of nnU-Net. This local fingerprint encloses the local dataset’s pixel intensity-based metrics, as well as spatial characteristics (such as spacing and voxel size) (see Table 1).

- **Global Fingerprint Aggregation:**

The nodes share their local fingerprint with the server, where these get aggregated to form a global fingerprint. Explicitly, the characteristics are aggregated as follows:

$$\hat{F} = \hat{f}k = g_k(f_k^i | i = 1^N) | k \in \mathcal{K} \quad (1)$$

where \hat{F} denotes the aggregated fingerprint, f_k^i represents the $k - th$ fingerprint key from node i , and g_k is the corresponding aggregation function. Table 1 lists the corresponding g_k functions for each fingerprint key. The *weighted_mean* is calculated with weights proportional to data samples quantity from each participating node.

Fig. 1 showcases an overview of the FFE process pipeline. As a final step, each node calculates its own nnU-Net training plan based on the received global fingerprint and local hardware characteristics. This process ensures that all nodes will be optimizing either highly compatible or, in most cases, identical network architectures (if the default nnU-Net’s memory constraint has not been altered between nodes).

2.3. Asymmetric Federated Averaging

In scenarios where nnU-Net is deployed across federated nodes, variations in model architecture can arise due to differences in data characteristics or computational capabilities. To address this inherent heterogeneity, we extend the classical FedAvg approach by developing an Asymmetric Federated Averaging strategy (AsymFedAvg). This method enables nodes to share only the parts of the model that have a common space with the rest of the federation, effectively eliminating the need to constrain all nodes to a single, identical architecture.

At each participating node, we initialize nnU-Net’s adaptive configuration pipeline to generate node-specific U-Net architectures based on the locally extracted dataset fingerprints of the centers. A set of example configurations obtained for each data center is presented in Table 2.

Let $\mathcal{K} = 1, \dots, K$ be the set of participating nodes in the federation. For each node $k \in \mathcal{K}$ we define a local model state dictionary as:

$$S^k = (l_i^k, \theta_i^k) | i \in \mathcal{L}^k \quad (2)$$

where l_i^k represents the layer identifier, θ_i^k denotes the corresponding parameters for node k , and \mathcal{L}^k is the set of layers in node k ’s model.

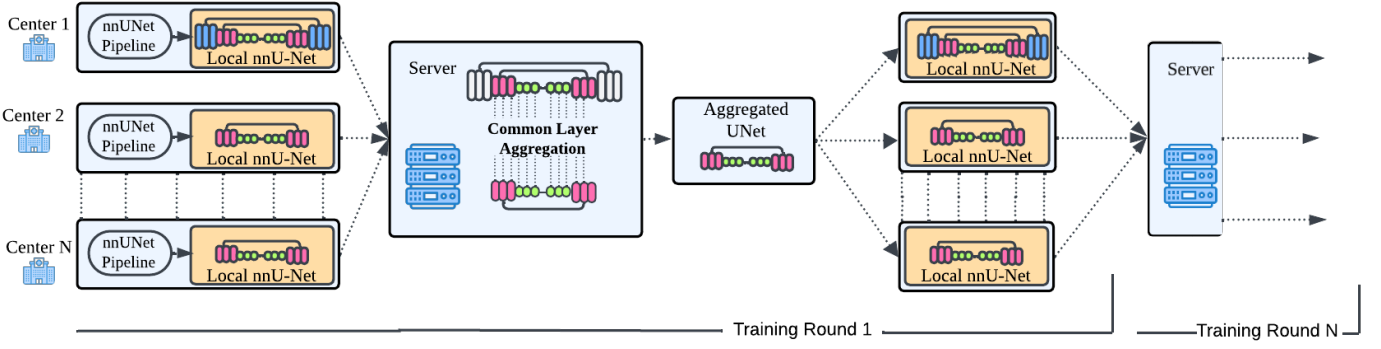


Figure 2: The Asymmetric Federated Averaging (AsymFedAvg) Pipeline process. The nodes of the federated setup generate a local nnU-Net from the nnU-Net pipeline. During training, the server receives the local nnU-Net weights of each node and aggregates them utilizing the Aggregation Function of AsymFedAvg. Finally, at the end of each training round, the server distributes the aggregated layers of the network back into the nodes. This process happens throughout the whole training.

We define a layer matching function \mathcal{C} which identifies the common layers of the models participating in the federation as:

$$\mathcal{C}(S_{k=1}^K) = \{l \mid \forall k, j \in \mathcal{K} : l \in \mathcal{L}^k \cap \mathcal{L}^j \wedge \dim(\theta_l^k) = \dim(\theta_l^j)\} \quad (3)$$

For each compatible layer $l \in \mathcal{C}(S_{k=1}^K)$, the aggregated parameters $\hat{\theta}_l$ are computed as:

$$\hat{\theta}_l = \frac{1}{|\mathcal{K}_l|} \sum_{k \in \mathcal{K}_l} \theta_l^k \quad (4)$$

where \mathcal{K}_l is the set of nodes that contain layers l .

The aggregated model state dictionary \hat{S} is then constructed as:

$$\hat{S} = (l, \hat{\theta}_l) \mid l \in \mathcal{C}(S^k, k = 1^K) \quad (5)$$

During each federation round t , the update process goes as follows:

Algorithm 1 Asymmetric Model Aggregation

- 1: Each node k sends its state dictionary S_t^k to the server
 - 2: The server identifies compatible layers using the matching function \mathcal{C}
 - 3: The server computes \hat{S}_t using the averaging procedure
 - 4: **for** each node k **do**
 - 5: **for** each layer l in model **do**
 - 6: **if** $l \in \mathcal{C}(\{S^k\}_{k=1}^K)$ **then**
 - 7: $\theta_{l,t+1}^k \leftarrow \hat{\theta}_l$
 - 8: **else**
 - 9: $\theta_{l,t+1}^k \leftarrow \theta_{l,t}^k$
 - 10: **end if**
 - 11: **end for**
 - 12: **end for**
-

The **AsymFedAvg** allows nodes to maintain their unique architectural components while sharing knowledge via their common space (compatible layers), handling the diverse nature of medical imaging data across different centers. Fig. 2 depicts an overview of the AsymFedAvg pipeline and the process of updating the heterogeneous architectures in each training round.

2.4. Implementation

2.4.1 Federated Learning Environment

For the federated communication, we select the Flower framework [24], which is an open-source library designed to streamline federated learning tasks on a cluster of machines. Flower’s high-level API eliminates the need for delving into complex and time-consuming processes such as network communication between nodes and model aggregation, as it already supports multiple FL optimization algorithms such as Federated Averaging (FedAvg), FedProx [25] and Federated SGD (FedSGD) [14].

Additionally, Flower’s client-server architecture is well-suited for our multi-center setup, as it allows seamless integration of local models while maintaining centralized coordination on the server.

Table 3: Hardware specifications of the computational nodes.

Node	CPU (Cores/GHz)*	GPU (Memory)**	OS ***
Node 1	i7-8700K (12/3.20)	GTX 1080 (8GB)	Ubuntu 22.04
Node 2	i7-8700K (12/3.20)	GTX 1080 (8GB)	Windows 10
Node 3	i7-9700K (8/3.60)	RTX 2080S (8GB)	Ubuntu 22.04
Node 4	i7-9700 (8/3.00)	RTX 2080S (8GB)	Ubuntu 22.04

*GPU: Graphics Processing Unit, **CPU: Central Processing Unit, ***OS: Operating system

2.4.2 FednnU-Net

Our framework maintains full functionality of the original nnU-Net while offering a federated extension that allows experimentation in both real and simulated environments. Its modular structure enables seamless integration not only with the original nnU-Net but also with its customized versions, allowing researchers to adapt their traditional centralized training methods to a federated setup.

2.4.3 Distributed Setup

Our experimental framework consists of 4 computational nodes with varying hardware and system specifications (Table 3), resembling real-world clinical scenarios in low-resource countries. In particular, the availability of GPU device with 8GB of memory, is the requirement for each node in order to run the default nnU-Net training setup. The proposed framework was deployed and tested independently across all nodes, although the final model training is done on a single, multi-GPU cluster to simplify experimental control.

3. Datasets

We evaluate our proposed methods on three distinct clinical applications, using datasets that serve as valuable testbeds due to their multi-institutional and heterogeneous cohorts. The following sections provide a detailed description of the datasets employed in each use case.

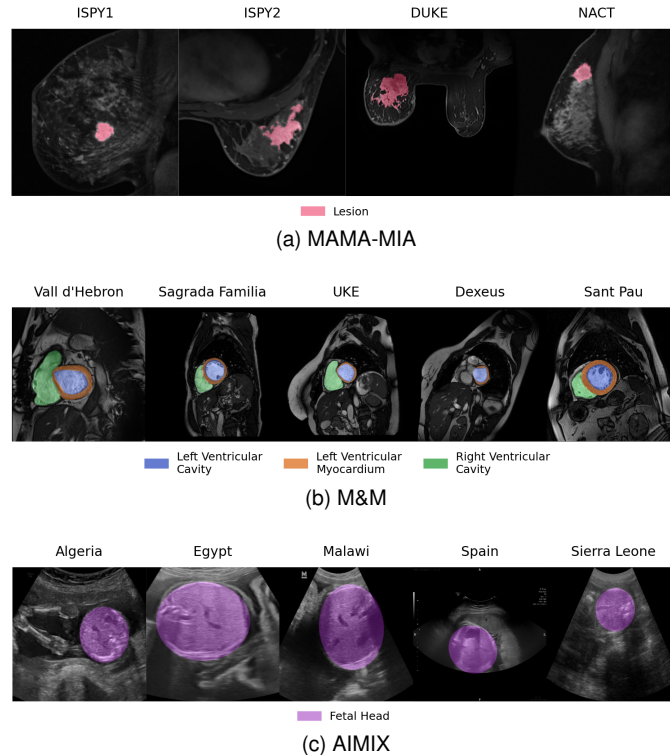


Figure 3: Example images with annotations from each data center used in the study.

3.1. Breast MRI

3.1.1 MAMA-MIA

The MAMA-MIA dataset [26] is the largest publicly available collection of breast dynamic contrast-enhanced MRI (DCE-MRI) cases with expert primary tumor segmentations, providing an essential resource for advancing and benchmarking AI algorithms in breast cancer imaging. It comprises 1,506 cases acquired between 1995 and 2016 from four cohorts within The Cancer Imaging Archive (TCIA): ISPY-1 (n=171), ISPY-2 (n=980), Duke (n=291), and NACT (n=64). The

Table 4: Summary of MRI acquisition parameters across the four centers (ISPY1, ISPY2, DUKE, and NACT) in the MAMA-MIA breast cancer dataset [26].

Center	Vendor	Scanner Model	Slice Thickness (mm)	Number of Slices	Field Strength (T)	Number of Studies
ISPY1	GE (67.3%)	Signa Genesis (60.2%) Other (39.8%)	2.4 [1.5, 4.0]	64 [44, 256]	1.5 (100.0%) 3.0 (0.0%)	171
	Siemens (25.7%)					
	Philips (7.0%)					
ISPY2	GE (62.3%)	Signa HDxt (54.7%) Avanto (12.6%) Other (32.7%)	2.0 [0.8, 3.0]	106 [52, 256]	1.5 (73.0%) 3.0 (27.0%)	980
	Siemens (25.7%)					
	Philips (11.9%)					
DUKE	GE (60.5%)	Other (55.7%) Avanto (24.1%) Signa HDxt (20.3%)	1.1 [1.0, 2.5]	169 [60, 256]	1.5 (46.7%) 3.0 (53.3%)	291
	Siemens (39.5%)					
NACT	GE (100%)	Signa Genesis (100%)	2.0 [2.0, 2.4]	60 [46, 64]	1.5 (100.0%) 3.0 (0.0%)	64

Table 5: Summary of MRI acquisition parameters across the three centers (GUMED, KAUNO, and HCB) in the EuCanImage breast MRI dataset.

Center	Vendor	Scanner Model	Slice Thickness (mm)	Pixel Spacing (mm)	Field Strength (T)	Number of Studies
GUMED (Poland)	Siemens	Aera (100%)	1.00–1.49	1.00–1.49	1.5 (100%)	30
KAUNO (Lithuania)	Philips (88.4%)	Ingenia (88.4%)	1.50–1.99 (84.5%)	0.50–0.99 (96.6%)	1.5 (11.6%)	232
	Siemens (11.6%)	Avanto (11.6%)			3.0 (88.4%)	
HCB (Spain)	GE (69.2%)	Signa HDxt (63.8%) Aera (22.8%) Others (13.4%)	2.00–2.49 (87.2%)	0.50–0.99 (98.1%)	1.5 (90.7%)	312
	Siemens (30.8%)				3.0 (9.3%)	

annotation process focused on delineating primary tumors and non-mass-enhanced lesions within a single breast, using the first post-contrast phase as the reference—a phase typically associated with maximum enhancement of cancerous tissues that offers superior contrast between lesions and surrounding healthy tissue compared to later phases. However, significant imaging differences among these cohorts (Table 4) pose challenges for training robust models. For example, the NACT cohort predominantly features scans with a 2 mm slice thickness and an average of 60 slices per case, whereas Duke’s samples are mostly acquired with 1 mm thickness and include an average of 169 slices per case. Moreover, the centers used different scanner models and field strengths, further contributing to the variability in imaging protocols.

3.1.2 EuCanImage:

Through the European project EuCanImage¹, we access a non-public breast MRI collection comprising 574 samples from three different countries. The EuCanImage dataset represents a multi-institutional effort to create standardized imaging biobanks for cancer research and serves here as an external test set to validate our methodology on data acquired under protocols that differ markedly from those in MAMA-MIA. Detailed specifications of the acquisition parameters are provided in Table 5. Notably, while MAMA-MIA includes both axial and sagittal acquisitions, the EuCanImage collection consists exclusively of axial slices. In addition, images in EuCanImage are predominantly acquired from scanner models that differ from those represented in MAMA-MIA, and a significantly larger fraction of the scans are captured at 3T field strength. Although the spatial image characteristics are largely similar between the two datasets, these differences in scanner models, field strengths, and imaging orientations lead to distinct scan appearances, potentially challenging the robustness of segmentation algorithms.

3.2. Cardiac MRI

3.2.1 M&Ms

To further validate our approach, we leverage the Multi-center, Multi-vendor & Multi-disease (M&Ms) cardiac MRI datasets. As a part of our study, we curate a merged version of datasets that were used in the M&Ms challenges [27]; [28] by excluding the overlapping samples based on anonymized patient IDs provided by each institution. This curation allows to reach the full potential of this data collection without the risk of replicated samples. The final, accumulated set consists of 543 unique, short-axis cardiac MRI scans with expert annotations from 5 distinct institutions. We make this collection publicly available². The M&Ms datasets are particularly valuable for validation due to their inherent heterogeneity (Table 6), they include images from four different vendors (Siemens, GE, Philips, Canon), various scanner models (from older systems like Symphony to newer ones like Vantage Orian), and different field strengths (1.5T and

¹<https://eucanimage.eu/>

²This data resource will be released upon the acceptance of this article.

Table 6: Average specifications of images acquired in different centers across the merged collection of M&Ms 1 [27] and M&Ms 2 [28] challenge datasets.

Center	Vendor	Scanner Model	Slice Thickness (mm)	Number of Slices	Field Strength (T)	Number of Studies
Hospital Vall d’Hebron	Siemens	Symphony TIM (63.18%) Avanto Fit (15.48%) Other (21.34%)	9.5	13	1.5 (97.91%) 3.0 (2.09%)	239
Clinica Sagrada Familia	Philips	Achieva	10	13	1.5	98
Universitätsklinikum Hamburg-Eppendorf	Philips	Achieva	10	11	1.5	51
Hospital Universitari Dexeus	GE	Signa Excite (75.24%) Signa HDxt (23.81%) Signa Explorer (0.95%)	9.9	12	1.5 (88.57%) 3.0 (11.43%)	105
Hospital Sant Pau	Canon	Vantage Orian	10	13	1.5	50

Table 7: Summary of the AIMIX and ACOUSLIC-AI datasets, including number of samples, mean resolution, nnU-Net patch size, and UNet stages for each dataset.

Center	Mean Resolution (h x w)	Number of Studies
Algeria	418x500	25
Egypt	450x400	20
Malawi	400x500	25
Spain	1228x1276	60
SierraLeone (External)	561x743	178

3.0T). This multi-center, multi-vendor nature mirrors the real-world variability in clinical settings, making these datasets ideal for testing the generalizability of our approach.

The technical heterogeneity across centers is evident in variations of scanner models, field strengths and different acquisition protocols. This diversity presents similar challenges to those encountered in our MAMA-MIA analysis, particularly in terms of standardization and harmonization of imaging parameters.

3.2.2 ACDC:

The Automated Cardiac Diagnosis Challenge (ACDC) dataset consists of 150 cardiac short-axis MRI examinations acquired at the University Hospital of Dijon (France) [3]. The dataset is evenly distributed across five groups (30 cases each): normal subjects (NOR), patients with myocardial infarction (MINF), dilated cardiomyopathy (DCM), hypertrophic cardiomyopathy (HCM), and abnormal right ventricle (RV). This dataset is particularly valuable for validation due to its well-defined pathological diversity and standardized acquisition protocols. It is used for external validation of models trained on M&Ms dataset.

3.3. Fetal Ultrasound

3.3.1 AIMIX

With a focus on resource-constrained environments, the **AIMIX**³ dataset was developed to advance inclusive image analysis in prenatal care. This dataset addresses critical challenges, including the scarcity of African medical data, limited computational resources, and a lack of clinical expertise. The dataset comprises pregnancy blind-sweeps 2D ultrasound scans, along with associated patient metadata such as age and ethnicity. The data span multiple international sites, including **Algeria, Egypt, Malawi and Spain**, reflecting diverse geographic and healthcare settings.

In this study, we focus on abdominal segmentation, a crucial step in prenatal ultrasound analysis. To enable the evaluation on this multi-center dataset, we provide a set of 130 standard-plane images with masks corresponding to the fetal abdomen⁴. Our data processing workflow involved detecting the optimal abdominal plane from the each blind-sweep and segmenting it using a 4-point ellipse-fitting algorithm [29], utilizing a semi-automatic software by a researcher with more than five years of experience and reviewed by an expert clinician. Table 7 lists the number of samples and the mean resolution for each center.

3.3.2 ACOUSLIC-AI Sierra Leone:

For the external validation, we utilize the publicly available samples from **ACOUSLIC-AI**⁵ Challenge dataset [30]. We use a collection of 178 cases collected in Sierra Leone from three Public Health Units (PHUs). With a resolution of

³<https://aimix-erc.eu/>

⁴This data resource will be released upon the acceptance of this article.

⁵<https://acouslic-ai.grand-challenge.org/datasets/>

Table 8: Quantitative results for multi-center MAMA-MIA and EuCanImage datasets. HD95 values reported in *mm*. Best results for privacy-preserving methods are in bold.

Method	ISPY1		ISPY2		DUKE		NACT		external GUMED		external KAUNO		external HCB	
	DSC ↑	HD95 ↓	DSC ↑	HD95 ↓	DSC ↑	HD95 ↓	DSC ↑	HD95 ↓						
Single-center	0.612	17.60	0.739	19.03	0.616	33.56	0.551	23.24	0.579	35.64	0.636	31.72	0.544	46.30
AsymFedAvg	0.634	16.69	0.739	18.15	0.621	28.70	0.620	21.79	0.557	51.43	0.637	32.43	0.551	49.10
FFE	0.644	16.20	0.742	17.48	0.653	39.54	0.660	17.49	0.582	28.83	0.645	33.52	0.565	40.41
Centralized	0.654	17.28	0.750	19.84	0.657	58.99	0.675	17.35	0.582	52.44	0.644	41.17	0.569	57.98

Table 9: Quantitative results for multi-center M&Ms and ACDC datasets. HD95 values reported in *mm*. Best results for privacy-preserving methods are in bold.

Method	Hospital Vall d’Hebron		Clinica Sagrada Familia		Universitätsklinikum Hamburg-Eppendorf		Hospital Dexeus		Hospital Sant Pau		external ACDC	
	DSC ↑	HD95 ↓	DSC ↑	HD95 ↓	DSC ↑	HD95 ↓	DSC ↑	HD95 ↓	DSC ↑	HD95 ↓	DSC ↑	HD95 ↓
Single-center	0.908	4.27	0.912	3.62	0.902	6.56	0.896	4.31	0.900	4.34	0.887	4.79
AsymFedAvg	0.909	4.20	0.913	3.70	0.907	4.23	0.897	4.29	0.902	4.07	0.889	4.58
FFE	0.911	4.05	0.914	3.67	0.922	3.30	0.904	3.98	0.904	3.87	0.897	3.87
Centralized	0.910	4.20	0.914	3.53	0.923	3.26	0.905	3.87	0.907	3.81	0.898	3.89

744×562 pixels, the images from Sierra Leone sit between the low-end devices used in Algeria and Malawi and the high-end scanners employed in Spain. This intermediate imaging quality makes the dataset an ideal candidate for assessing model generalizability across varying image qualities and clinical environments, ensuring robust validation of AI performance.

4. Experiments

4.1. Experimental setups

The training process is conducted across four different setups:

- **Single-center Training:** Each node independently trains its own nnU-Net model using only its local dataset. This setup serves as a baseline, reflecting the performance of a node/institution without participation in the federation.
- **Centralized Training:** All data is aggregated into a single dataset, which is used to train a centralized model. This setup represents the theoretical upper bound of performance, though it is typically infeasible in real-world scenarios due to privacy constraints.
- **Federated Fingerprint Training:** Utilizing our FFE approach (2), the local dataset fingerprints from all nodes are aggregated at the central node into one federated fingerprint and distributed back to each node. As a result, each training site obtains identical network architecture during the nnU-Net’s self-configuration process. This approach approximates the nnU-Net’s behavior in the centralized training setup.
- **Asymmetric Aggregation Training:** Implemented using our **AsymFedAvg** strategy, allowing nodes to maintain their original nnU-Net configured architectures while sharing compatible parts of their networks.

For our experimentation, we maintain nnU-Net’s default configuration parameters as described in [7]. We test the 2D U-Net architecture on breast MRI and fetal ultrasound data and the 3D architecture on a cardiac MRI use case, consistently employing the default training length of 1000 epochs and using the last model checkpoint for evaluation across all federated nodes. Following other recent works on medical image segmentation [7, 31–33], we evaluate the models with Dice Similarity Coefficient (DSC) and 95% Hausdorff distance (HD95). For internal validation, we report results as the average of a 5-fold cross-validation, while for external testing, we follow the original nnU-Net approach by generating ensemble predictions from all five folds. Moreover, each experiment uses identical data splits—for example, the *n*-th fold in the centralized setup corresponds directly to the set of *n*-th folds from centers used in the local setup. By adhering to these protocols, we try to minimize the influence of other factors on the final results, ensuring that any observed performance variations are primarily due to our federated learning adaptations rather than modifications to the base framework.

4.2. Results

4.2.1 Breast MRI

Table 8 presents the segmentation performance for the breast lesion MAMA-MIA dataset. Both proposed methods, FFE and AsymFedAvg, outperform the local training of individual centers in terms of DSC and HD95 across all datasets. Specifically, FFE method achieves an average DSC improvement of 3.2% on ISPY1, 0.3% on ISPY2, 3.7% on DUKE, and a notable 10.9% on NACT. Additionally, FFE maintains DSC scores close to the centralized approach, while surpassing it in terms of HD95, effectively bridging the performance gap in a decentralized framework. Interestingly for

Table 10: Quantitative results for multi-center AIMIX and ACOUSLIC-AI datasets. HD95 values reported in *pixels* due to missing spacing information. Best results for privacy-preserving methods are in bold.

Method	Algeria		Egypt		Malawi		Spain		external Sierra Leone	
	DSC \uparrow	HD95 \downarrow	DSC \uparrow	HD95 \downarrow						
Single-center	0.952	11.87	0.931	24.21	0.926	26.83	0.942	29.82	0.831	53.20
AsymFedAvg	0.951	11.16	0.941	18.29	0.939	16.20	0.944	25.42	0.851	43.44
FFE	0.955	10.23	0.954	14.56	0.943	15.64	0.938	47.58	0.809	46.57
Centralized	0.954	10.23	0.953	14.50	0.943	15.55	0.932	55.76	0.804	54.34

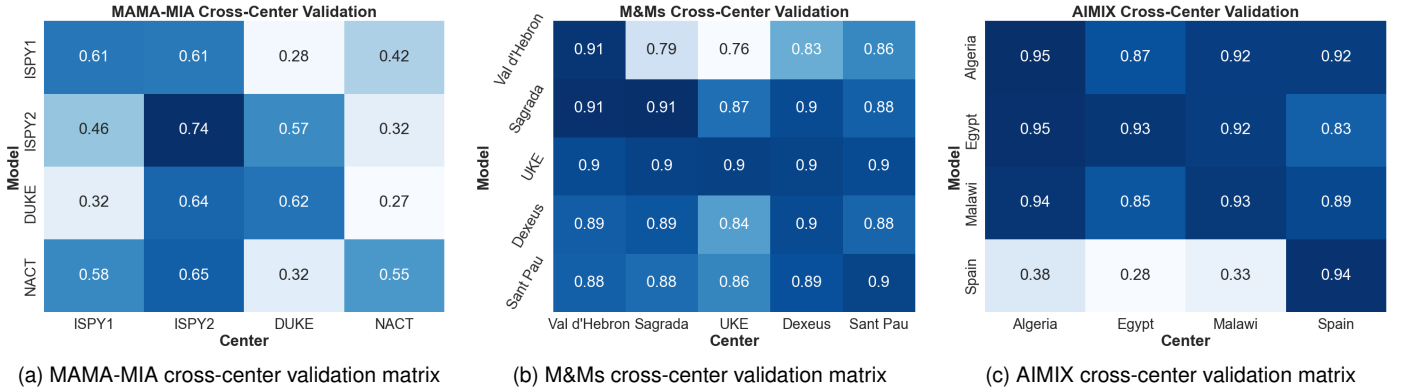


Figure 4: Cross-center DSC scores for isolated model training predictions across multiple centers.

DUKE, AsymFedAvg outperforms every other method in terms of HD95. Since the DUKE dataset comprises samples of substantially different spatial characteristics (pixel resolution approximately 2 times higher, see Table 4), the adaptive nature of the asymmetric aggregation approach allows this center to maintain its initial architecture, while benefiting from the other centers. In this case, the HD95 gets reduced in contrast to unified architecture methods (FFE and centralized setting). The cross-center validation matrix in Fig. 4 further exposes the dataset’s heterogeneity, where both ISPY2 and NACT trained models struggle to generalize well for the DUKE dataset, with the only exception of ISPY2, which has image resolution much closer to DUKE. Sample predictions presented in Fig. 5 show the strong improvement of segmentation performance for NACT dataset, which struggles to perform well with its locally trained nnU-Net model. For DUKE, HD95 improvement can be observed for AsymFedAvg model prediction. External validation results for the EuCanImage dataset show that federated training with the FFE method achieves DSC scores on par with the centralized model. While the segmentation performance for the KAUNO center is comparable to the results achieved within MAMA-MIA dataset, demonstrating good generalizability. The GUMED center exhibits a notable decrease in performance, which is most likely attributed to discrepancies in annotation protocols rather than the data itself. An example of such difference is illustrated in Fig. 7, where fine-grained model predictions fail to align with coarse ground truth regions provided by experts.

4.2.2 Cardiac MRI

For M&Ms, similarly to previous dataset, both proposed federated learning methods outperform the local, non-collaborative training setup across both tested metrics. The only exception being Clinica Sagrada Familia, for which the HD95 is lower in the local setup by a minimal margin. FFE method consistently achieves the highest scores in terms of DSC for both internal and external datasets, while the adaptive AsymFedAvg does not reflect substantial benefits from federated training. Most likely, it is caused by dominantly homogeneous nature of M&Ms dataset, in which all data centers share similar sample characteristics making a common architecture method more suitable. This effect can be observed as well in the cross-center evaluation of locally trained models (see Fig. 4) where each center managed to provide acceptable results for samples from other, unseen institutions. Moreover, it is important to note that the FFE method, despite the additional privacy requirement manages to provide almost identical performance to the centralized training scenario. Sample predictions for cardiac MRI dataset can be observed in Fig. 6. All tested methods provide consistent results for central slices while having more visible disparities in regions close to the heart’s apex (sample predictions from ACDC) and heart’s atria (sample predictions from Vall d’Hebron).

4.2.3 Fetal Ultrasound

For fetal abdomen segmentation task, considerable differences can be observed between FFE and AsymFedAvg methods; see Table 10. Due to strong data heterogeneity, i.e. discrepancies in capture devices and image resolution between centers (Table 7), the models trained with data from Algeria, Egypt or Malawi do not generalize well for higher resolution samples from Spain; see Fig. 4c. In this case, having a unified training strategy for all centers does not prove to be the

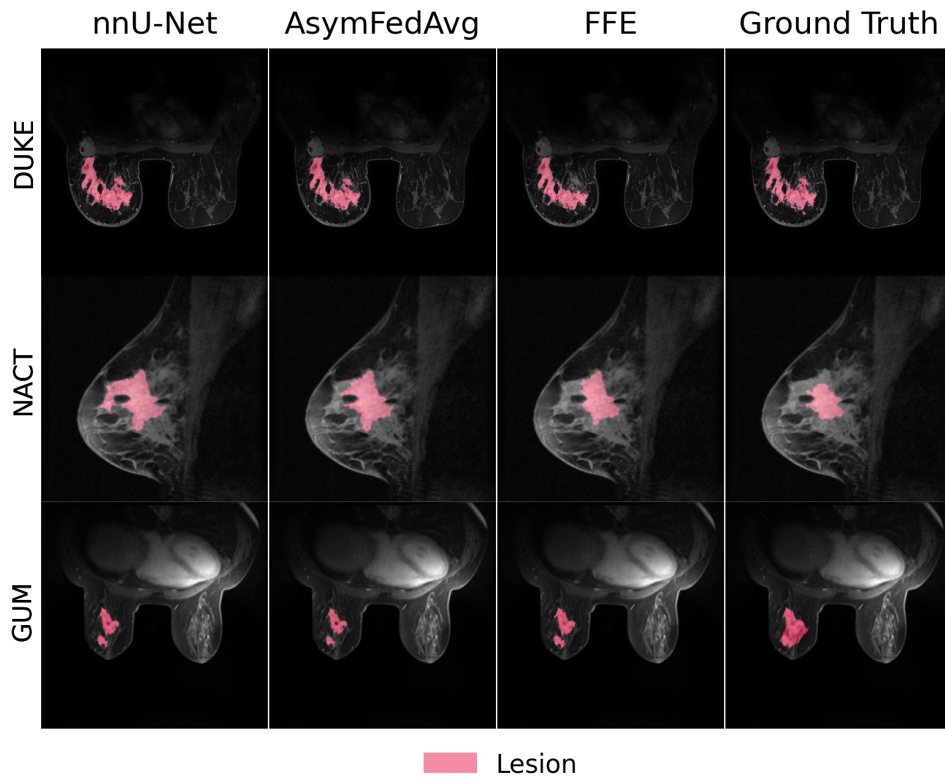


Figure 5: Sample predictions of each method for Breast Cancer datasets.

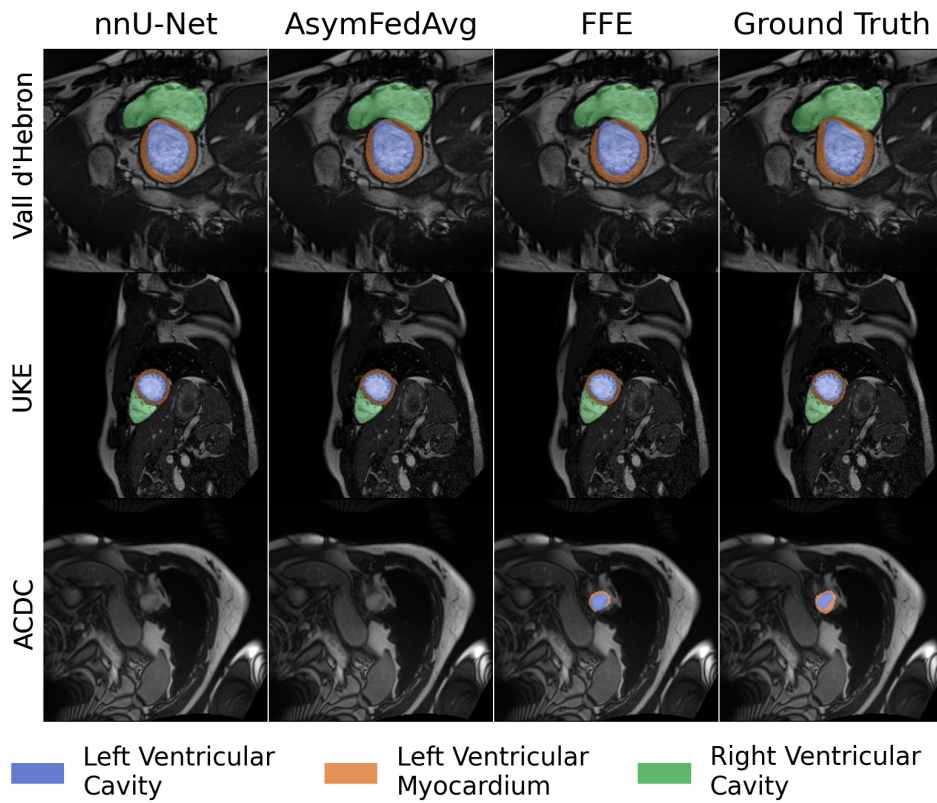


Figure 6: Sample predictions of each method for cardiac MRI datasets.

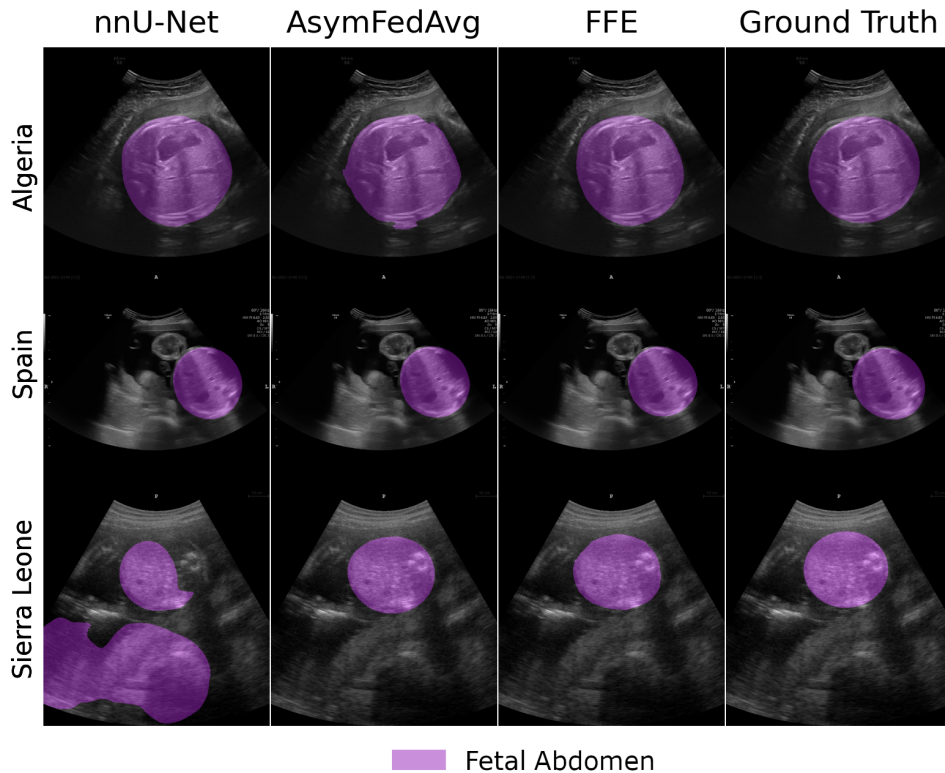


Figure 7: Sample predictions of each method for AIMIX dataset.

optimal solution. Allowing the largest center, i.e. Spain, to keep its original architecture allows to get a more appropriate model to the characteristics of the external center, i.e. Sierra Leone, while still benefiting from the federated training and contribution of other centers. This effect can be observed on sample predictions presented in Fig. 7. The single-center nnU-Net model often struggled to identify the right region for abdomen delineation, which can be especially observed in the external validation samples from Sierra Leone.

5. Discussion

Our experiments across three diverse imaging use cases - breast MRI (MAMA-MIA), cardiac MRI (M&Ms), and fetal ultrasound (AIMIX) - show that FednnU-Net can reliably match, or even surpass conventional centralized strategies. These results add to a growing body of evidence illustrating that distributed model optimization can achieve comparable accuracy while respecting the complexities of real-world clinical collaborations, such as data privacy and varied institution-specific protocols. Moreover, our findings underscore the critical need for methods that effectively handle data heterogeneity during federated model training.

Whilst other, federated state-of-the-art segmentation methods may achieve higher accuracy with highly customized solutions for specific tasks, the primary objective of this work is to provide an easy-to-use, privacy-preserving solution accessible to researchers with varying levels of expertise. In doing so, we prioritize the broader applicability and real-world viability of the framework over achieving the absolute highest segmentation performance.

The increasing emphasis on privacy-preserving, decentralized settings is rapidly becoming the standard in modern AI solutions — especially within healthcare, where patient data confidentiality is paramount. FednnU-Net aligns with this trend by enabling collaborative training without compromising data privacy. However, several aspects require further investigation:

1. **Scalability and Client Diversity:** Future studies should test FednnU-Net with a larger number of nodes to better mimic real-world deployments, where numerous and geographically dispersed institutions may challenge model convergence and communication.
2. **Heterogeneous Computational Resources:** Given that clients often have different processing capabilities, it is crucial to evaluate FednnU-Net under varied hardware constraints. Although our framework already supports such a scenario, this dimension was not explored in this current study.
3. **Enhanced Privacy Mechanisms:** Beyond our current privacy measures, integrating techniques such as differential privacy [34, 35] and secure multiparty computation (SMPC) could further reduce the risk of data leakage, even in aggregated updates.

In summary, although more accurate medical segmentation techniques exist, FednnU-Net fills a vital gap by balancing segmentation performance with ease-of-use and privacy preservation. As federated learning continues to mature and becomes an increasingly standard practice in healthcare, addressing these limitations through further evaluation and enhancements will be essential for broader adoption and improved robustness in clinical applications.

6. Conclusion

In this study, we present FednnU-Net, a federated learning framework for 2D and 3D medical image segmentation that bridges the gap between privacy-sensitive setups and high-performance model training. Our framework introduces two methods: Federated Fingerprint Extraction (FFE) and Asymmetric Federated Averaging (AsymFedAvg) that unlock the potential of distributed model training under privacy constraints. FFE enables construction of one, universal model architecture akin to centralized training, ensuring robustness across data centers. Alternatively, AsymFedAvg allows tailored model customization for each center to better align with local data characteristics. Our results demonstrate that both FFE and AsymFedAvg offer distinct performance benefits depending on the multi-center dataset characteristics, either achieving performance close to the centralized setting or surpassing it, particularly in highly diverse datasets. On top of that, both approaches preserve nnU-Net’s hallmark self-configuring capabilities, and due to our modular open-source implementation, they allow researchers to seamlessly translate their nnU-Net-derived centralized segmentation methods to the federated setting. Furthermore, we open source our framework and release data enhancing two public dataset collections to allow reproducibility of results. We hope that our contributions provide a robust foundation for further development and evaluation of medical image segmentation models in privacy-constrained settings.

References

- [1] A. Reza *et al.*, “Medical image segmentation review: The success of u-net,” *IEEE Transactions on Pattern Analysis and Machine Intelligence*, 2024.
- [2] X. Yang *et al.*, “A medical image segmentation method based on multi-dimensional statistical features,” *Frontiers in Neuroscience*, vol. 16, 09 2022.
- [3] O. Bernard *et al.*, “Deep learning techniques for automatic mri cardiac multi-structures segmentation and diagnosis: Is the problem solved?,” *IEEE Transactions on Medical Imaging*, vol. 37, no. 11, pp. 2514–2525, 2018.
- [4] N. Stanislav *et al.*, “Deep learning to achieve clinically applicable segmentation of head and neck anatomy for radiotherapy.” arXiv: 1809.04430.
- [5] T. C. Hollon *et al.*, “Near real-time intraoperative brain tumor diagnosis using stimulated raman histology and deep neural networks,” *Nature medicine*, vol. 26, pp. 52–58, 2020.
- [6] E. Morteza, S. A. Line, B. E. Magnus, S. Ole, and R. Ingerid, “The direction of tumour growth in glioblastoma patients,” *Scientific reports*, vol. 8, no. 1, p. 1199, 2018.
- [7] F. Isensee, P. F. Jaeger, S. A. A. Kohl, J. Petersen, and K. H. Maier-Hein, “nnu-net: a self-configuring method for deep learning-based biomedical image segmentation,” *Nature Methods*, vol. 18, pp. 203–211, 2 2021.
- [8] J. Ma, “Cutting-edge 3d medical image segmentation methods in 2020: Are happy families all alike?.” arXiv: 2101.00232, 2021.
- [9] F. Isensee *et al.*, “ nnU-Net Revisited: A Call for Rigorous Validation in 3D Medical Image Segmentation ,” in *proceedings of Medical Image Computing and Computer Assisted Intervention – MICCAI 2024*, vol. LNCS 15009, Springer Nature Switzerland, October 2024.
- [10] O. Ronneberger, P. Fischer, and T. Brox, “U-net: Convolutional networks for biomedical image segmentation,” in *Medical image computing and computer-assisted intervention–MICCAI 2015: 18th international conference, Munich, Germany, October 5-9, 2015, proceedings, part III 18*, pp. 234–241, 2015.
- [11] B. Liang *et al.*, “Automatic segmentation of 15 critical anatomical labels and measurements of cardiac axis and cardiothoracic ratio in fetal four chambers using nnu-netv2,” *BMC Med. Inform. Decis. Mak.*, vol. 24, 05 2024.
- [12] Y. Choi, J. Bang, S.-Y. Kim, M. Seo, and J. Jang, “Deep learning–based multimodal segmentation of oropharyngeal squamous cell carcinoma on ct and mri using self-configuring nnu-net,” *European Radiology*, vol. 34, no. 8, pp. 5389–5400, 2024.
- [13] L. Huang, A. Miron, K. Hone, and Y. Li, “ Segmenting Medical Images: From UNet to Res-UNet and nnUNet ,” in *2024 IEEE 37th International Symposium on Computer-Based Medical Systems (CBMS)*, (Los Alamitos, CA, USA), pp. 483–489, IEEE Computer Society, June 2024.
- [14] H. B. McMahan, E. Moore, D. Ramage, S. Hampson, and B. A. y Arcas, “Communication-efficient learning of deep networks from decentralized data,” in *International Conference on Artificial Intelligence and Statistics*, 2016.
- [15] E. Diao, J. Ding, and V. Tarokh, “Heterofl: Computation and communication efficient federated learning for heterogeneous clients.” arXiv: 2010.01264, 2021.
- [16] X. Fang and M. Ye, “Noise-robust federated learning with model heterogeneous clients,” *IEEE Transactions on Mobile Computing*, 2024.
- [17] N. Koutsoubis, Y. Yilmaz, R. P. Ramachandran, S. Matthew, and R. Ghulam, “Privacy preserving federated learning in medical imaging with uncertainty estimation.” arXiv: 2406.12815, 6 2024.
- [18] Y. Zheng, P. Tang, T. Ju, H. Wang, W. Qiu, and J. C. Rajapakse, “Federated semi-supervised learning for medical image segmentation with intra-client and inter-client consistency,” in *2024 IEEE International Conference on Bioinformatics and Biomedicine (BIBM)*, pp. 4054–4059, 2024.
- [19] Y. Xia *et al.*, “Auto-fedavg: Learnable federated averaging for multi-institutional medical image segmentation.” arXiv: 2104.10195, 4 2021.
- [20] G. Sun, H. Shu, F. Shao, T. Racharak, W. Kong, Y. Pan, J. Dong, S. Wang, L.-M. Nguyen, and J. Xin, “Fkd-med: Privacy-aware, communication-optimized medical image segmentation via federated learning and model lightweighting through knowledge distillation,” *IEEE Access*, vol. 12, pp. 33687–33704, 2024.
- [21] H. Wu, B. Zhang, C. Chen, and J. Qin, “Federated semi-supervised medical image segmentation via prototype-based pseudo-labeling and contrastive learning,” *IEEE Transactions on Medical Imaging*, vol. 43, no. 2, pp. 649–661, 2024.

- [22] J. Wicaksana, Z. Yan, D. Zhang, X. Huang, H. Wu, X. Yang, and K.-T. Cheng, "Fedmix: Mixed supervised federated learning for medical image segmentation," *IEEE Transactions on Medical Imaging*, vol. 42, no. 7, pp. 1955–1968, 2023.
- [23] Y. Ma, J. Wang, J. Yang, and L. Wang, "Model-heterogeneous semi-supervised federated learning for medical image segmentation," *IEEE Transactions on Medical Imaging*, vol. 43, no. 5, pp. 1804–1815, 2024.
- [24] D. J. Beutel *et al.*, "Flower: A friendly federated learning research framework," *arXiv: 2007.14390*, 2020.
- [25] T. Li, A. K. Sahu, M. Zaheer, M. Sanjabi, A. Talwalkar, and V. Smith, "Federated optimization in heterogeneous networks," 2020.
- [26] L. Garrucho *et al.*, "A large-scale multicenter breast cancer DCE-MRI benchmark dataset with expert segmentations," 2024. *arXiv: 2406.13844*.
- [27] V. M. Campello *et al.*, "Multi-centre, multi-vendor and multi-disease cardiac segmentation: The m&ms challenge," *IEEE Transactions on Medical Imaging*, vol. 40, no. 12, pp. 3543–3554, 2021.
- [28] C. Martín-Isla *et al.*, "Deep learning segmentation of the right ventricle in cardiac mri: The m&ms challenge," *IEEE Journal of Biomedical and Health Informatics*, vol. 27, no. 7, pp. 3302–3313, 2023.
- [29] G. Carneiro, B. Georgescu, S. Good, and D. Comaniciu, "Detection and measurement of fetal anatomies from ultrasound images using a constrained probabilistic boosting tree," *IEEE Transactions on Medical Imaging*, vol. 27, no. 9, pp. 1342–1355, 2008.
- [30] M. S. Sappia *et al.*, "Acouslic-ai: Abdominal circumference operator-agnostic ultrasound measurement in low-income countries using artificial intelligence," 2024. under review.
- [31] A. Hatamizadeh *et al.*, "UNETR: Transformers for 3D Medical Image Segmentation," in *2022 IEEE/CVF Winter Conference on Applications of Computer Vision (WACV)*, (Los Alamitos, CA, USA), pp. 1748–1758, IEEE Computer Society, Jan. 2022.
- [32] T. Chen, C. Wang, Z. Chen, Y. Lei, and H. Shan, "Hidiff: Hybrid diffusion framework for medical image segmentation," *IEEE Transactions on Medical Imaging*, vol. 43, no. 10, pp. 3570–3583, 2024.
- [33] H.-Y. Zhou *et al.*, "nnformer: Volumetric medical image segmentation via a 3d transformer," *IEEE Transactions on Image Processing*, vol. 32, pp. 4036–4045, 2023.
- [34] C. Dwork, "Differential privacy," in *Automata, Languages and Programming* (M. Bugliesi, B. Preneel, V. Sassone, and I. Wegener, eds.), (Berlin, Heidelberg), pp. 1–12, Springer Berlin Heidelberg, 2006.
- [35] A. E. Ouadrhiri and A. Abdelhadi, "Differential privacy for deep and federated learning: A survey," *IEEE Access*, vol. 10, pp. 22359–22380, 2022.